Journal of Alloys and Compounds 509 (2011) 1601–1606

Contents lists available at ScienceDirect

Journal of Alloys and Compounds

journal homepage: www.elsevier.com/locate/jallcom

Synthesis and consolidation of TiN/TiB_2 ceramic composites via reactive spark plasma sintering

I. Khobta [a,*], O. Petukhov [a], O. Vasylkiv [b], Y. Sakka [b], A. Ragulya [a]

[a] Institute for Problems of Materials Science, National Academy of Science of the Ukraine, Kiev 03680, Ukraine
[b] National Institute for Materials Science, 1-2-1, Sengen, Tsukuba, Ibaraki 305-0047, Japan

ARTICLE INFO

Article history:
Received 13 August 2010
Received in revised form 28 October 2010
Accepted 29 October 2010
Available online 10 November 2010

PACS:
81.05.Je, Mh
81.07.Bc
81.20.Ev
81.70.Bt

Keywords:
Composite materials
Sintering
Mechanical properties
Microstructure
Scanning electron microscopy (SEM)
X-ray diffraction

ABSTRACT

The simultaneous synthesis and densification of TiN/TiB_2 ceramic composites via reactive spark plasma sintering (RSPS) was investigated. Different component ratios (TiH_2/BN (TiN, B)) and heating rates (112.5–300 °C/min) were used to initiate the chemical reaction for TiN/TiB_2 synthesis. The omit RSPS process was revealed to have three stages, which are described separately. The relationships between the RSPS conditions, the microstructure and the properties of sintered ceramic composites were established. A Vickers hardness of 16–25 GPa and a fracture toughness of 4–6.5 MPa $m^{1/2}$ were measured for various compositions. Sintered ceramic composites containing 36 wt% TiB_2 with the highest relative density of 97.4 ± 0.4% and an average grain size of 150–550 nm have been obtained.

1. Introduction

Design and processing of new materials with improved high temperature properties is one of the challenging tasks of modern engineering. Ceramic materials such as nitrides and borides are natural candidates for advanced structural applications due to their exceptional hardness and stability at very high temperatures. Titanium nitride (TiN) has excellent combination of physical properties (high melting point, high hardness, low electrical resistivity, and gold like color) and chemical and metallurgical stability (high corrosion resistance to acid and alkaline solutions) [1]. Titanium diboride (TiB_2) also exhibits many unique physical properties such as high hardness and strength retention, good electrical and thermal conductivities, high melting point, chemical stability, and high wear resistance [2,3]. Furthermore, the use of these ceramics in composites offers the advantages of enhanced fracture toughness and noncatastrophic failure mode [4,5]. Thus, TiN–TiB_2 ceramic composite (CC) could be attractive for application in jet engine parts, armor plates, cutting tools and dies as well as high performing electrical systems [4]. However, because of their extremely high melting points, consolidation of this powder composite requires high temperature and long holding times. These conditions adversely affect both microstructure, i.e. grain growth accompanies consolidation, and cost effectiveness of the production process [6].

Spark Plasma Sintering (SPS) [7,8], also known as Field-Assisted Sintering [9] or electric-discharge sintering [10,11] is a promising technique of powder consolidation. It enjoys certain inherent advantages, such as high thermo-efficiency, rapid heating-up, self-cleaning of the surface of particles and enhanced sintering activity, enabling fast densification under relative low temperatures [12]. Moreover, the possibility of high exothermic reactions initiation in self-propagating high-temperature synthesis (SHS) mode by means of SPS technology [13] is also an advantage of this method. Numerous experimental investigations [1,6,14–16] point to the ability of SPS to consolidate highly dense powder products with the potential of grain size retention. The latter ability is of significance for the consolidation of nanocomposites where the grain growth is one of the major problems. Until now, the SPS technology has been used to fabricate various materials including metals and alloys,

* Corresponding author at: Institute for Problems of Materials Science, National Academy of Science of the Ukraine, Krzhizhanovsky str., 3, 03680, Kiev-142, Ukraine. Tel.: +380 44 424 15 33; fax: +380 44 424 21 31.
E-mail address: hobta_igor@ipms.kiev.ua (I. Khobta).

0925-8388/$ – see front matter © 2010 Elsevier B.V. All rights reserved.
doi:10.1016/j.jallcom.2010.10.198

compounds, ceramics, composite, especially some bulk amorphous and nanomaterials, multi scaled structure and functionally graded materials, etc. [1,6,14–20].

In the present work, the simultaneous synthesis and densification of TiN–TiB_2 ceramic composites with different component ratios (20 wt%, 36 wt%, 60 wt% and 80 wt% of TiB_2) via reactive spark plasma sintering (RSPS) of ball milled/mixed reactants (TiH_2, BN, TiN and B) was investigated. At the same time, the influence of component ratios and heating rate on densification, grain growth, microstructure, physical and mechanical properties of TiN–TiB_2 ceramic composites during the RSPS process was also investigated.

2. Materials and methods

TiH_2 (12 μm, purity > 99%), BN (0.16 μm, purity > 93%), B (0.43 μm, purity > 96%) and TiN (0.07 μm, purity > 96%) powders were used as raw materials. Homogeneous powder mixtures of four different composition (all wt%) 41.2TiH_2–13.1BN–45.7TiN, 75.9TiH_2–24.1BN, 73.5TiH_2–14.9BN–11.6B and 71.6TiH_2–7.4BN–21B that corresponded to 20, 36, 60 and 80 wt% of TiB_2 in sintered composites were prepared by high energy ball milling/mixing for 2 h using ethanol and agate balls as milling media. CR (ball to powders weight ratio) equals to about 1.5 and rotation velocity of the jar–650 rpm. The specific surface area (S_{spec}) of the initial and milled/mixed powder mixtures were measured by express method of gas chromatography (GCh–1, Moscow, Russia).

The milled powder mixtures were put into a graphite die (10 mm inner diameter) and sintered with the Dr. Sinter® 1050 spark plasma sintering system (Sumitomo Coal Mining Co., Tokyo, Japan) in vacuum of 7.5×10^{-2} Torr. This unit makes it possible to record temperature, punch displacement profile, vacuum level, current and voltage in real time. The used DC pulse sequence is 12:2 implying that the current is ON during 12 pulses (3.3 ms each) and OFF during two time intervals. The temperature of the SPS process was monitored by a pyrometer that was focused on the surface of the die.

Initially, pressure of 60 MPa was applied in order to ensure the proper electric contact between powder tablet and the graphite die and then was increased to 80 MPa after 900 °C. The heating rate of 140 °C/min from room temperature up to 700 °C followed by ramping in the range 112.5–300 °C/min up to 1600 °C was controlled during the RSPS process. The total processing lasted for 12–17 min and the holding for 3 min at final temperature of sintering. After the sintering process, the samples was first allowed to cool with matrix and then removed from the die. The relative density of the composites was determined by Archimedes method using distilled water as wetting liquid.

Phase identification of both milled/mixed powder mixtures and SPSed composites were made by using XRD analysis (JEOL - JDX-3500, Tokyo, Japan) with Cu Kα radiation. The microstructure of milled/mixed powder mixtures and densified products was examined by scanning electron microscopy (SEM) (JEOL–JSM6490LV, Tokyo, Japan).

The hardness and fracture toughness (K_{IC}) were obtained from indentation experiments using a Vickers diamond indenter (Micromet, Buehler GmbH, Germany). The applied load was equal to 0.98 N and 19.6 N while the dwell time was 10 s. An equation derived by Palmquist was used to calculate K_{IC} [6,21]. For all the samples, the crack length to indentation half-diagonal ratio, a/l, was <2.3 which is within the empirical limits of Palmquist cracks, $a/l \leq 2.5$ [4,22].

3. Results and discussion

The recorded X-ray diffraction patterns of the milled/mixed powder mixtures revealed that no reaction took place between TiH_2 and BN (TiN, B), and therefore no new phases were formed. They also showed that none of the oxide phases that could have formed during the milling/mixing process were detected. Moreover, in the milled/mixed powder mixtures, no peaks were seen for boron, which is evidence that the boron has become amorphous.

According to the obtained S_{spec} data, the calculated average particle size of the milled/mixed powder mixtures was in the range of 100–300 nm and depended on the composition. However, the SEM observation revealed the formation of relatively coarse (2–4 μm) agglomerates of TiH_2 particles covered with a layer of ultrafine BN particles as a result of milling/mixing of the initial powders. The particles of nanocrystalline TiN and ultrafine B powders were randomly distributed throughout the volume of the powder mixtures.

Diagrams presenting the shrinkage profile ($\Delta L/L$) and the change in the temperature and vacuum level of the system during RSPS were obtained for all compositions and sintering regimes. For instance, the process for the sample containing 36 wt% TiB_2 and sintered with a heating rate of 225 °C/min is illustrated in Fig. 1(a). As can be seen, the consolidation process is divided into three stages.

Stage 1 is hydrogen release at temperatures above 180 °C. This stage corresponds to the removal of the first portion of hydrogen (adsorbed and dissolved) in accordance with the equation $TiH_2 \rightarrow TiH_{2-x} + xH\uparrow$. The evidence of this is the decrease in the system vacuum level (Fig. 1(a)). According to [23], the calculated mean free path for atomic hydrogen depends on the hydrogen particle pressure over the TiH_2 surface, and at a temperature in the range of 200–960 °C varies in the interval of 2.37–11.9 mm. This distance considerably exceeds the gap between particles of TiH_2 and BN (TiN, B). In the first stage, reactions do not proceed until 800 ± 15 °C. In this stage, no significant change in shrinkage was observed.

Stage 2 involves chemical reactions in the system during the most intensive dehydrogenation process. This process is characterized by two peaks overlapping in the range of 800–1300 °C. The temperature marking the start of the second stage varies within $T_2 \approx 785$–835 °C and depends on the composition of CCs (Fig. 1(a), Table 1). The synthesis of the TiN–TiB_2 ceramic composite starts from a TiH_2–BN (TiN, B) mixture and proceeds in accordance with the following overall chemical reactions [5,24,25]:

$$3TiH_2 + 2BN \rightarrow 2TiN + TiB_2 + 3H_2(6H)\uparrow, \quad (1)$$

$$2TiH_2 + BN + B \rightarrow TiN + TiB_2 + 2H_2(4H)\uparrow. \quad (2)$$

The atomic hydrogen released from TiH_2 during the first and second stages favors BN decomposition accompanied by the formation of boranes and atomic nitrogen following to the reaction

$$2BN + 6H \rightarrow B_2H_6 + 2N\uparrow. \quad (3)$$

The active elemental titanium (the product of TiH_2 dehydrogenation) reacts with atomic nitrogen, forming the initial TiN phase that was identified by XRD in an additional experiment. The subsequent decomposition of stable and unstable boranes is accompanied by the formation of active atomic boron, which later reacts with titanium, giving the TiB_2 phase as well as secondary hydrogen:

$$B_2H_6 \rightarrow 2B + 3H_2(6H)\uparrow. \quad (4)$$

The possibility of a simultaneous solid-state reaction between titanium and boron nitride at elevated temperatures and that of contact between particles cannot be excluded. It should be noted that the dehydrogenation of TiH_2 is completed at a temperature of about 900–960 °C (peak *a* in Fig. 1(a)). Moreover, the dehydrogenation peak coincides with the greater shrinkage rate in the second stage ($d(\Delta L/L)/dt$ in Fig. 1(a)) and, thus, with the highest reaction rate. Peak *b* (the second drop in the vacuum level) is evidence of the formation of secondary hydrogen in accordance with reaction (4).

Stage 3 is direct sintering of the synthesized TiN and TiB_2 components. As can be seen in Fig. 1(b), the temperature marking the start of the third stage (T_3) increases from 1300 to 1505 °C with increasing TiB_2 content in sintered CCs (Table 1). This occurs as a result of the exothermic reaction between titanium and boron, which can inhibit the synthesis process under conditions approaching adiabatic ones. The reason for the lower temperature in the third stage for CCs containing 20 wt% TiB_2 is the addition of inert nanocrystalline TiN to the initial powder mixture that is not involved in the synthesis process and the densification of which occurs earlier. It should be noted that the heating rate has no significant effect on the temperature of the start of the stages described above (Table 1).

Typically, increasing the heating rate within an interval of 112.5–300 °C/min and the TiB_2 content in the sintered CCs leads to an increase in the maximal shrinkage for the investigated compositions (Fig. 1(b)). This is a result of the self-heating of the system

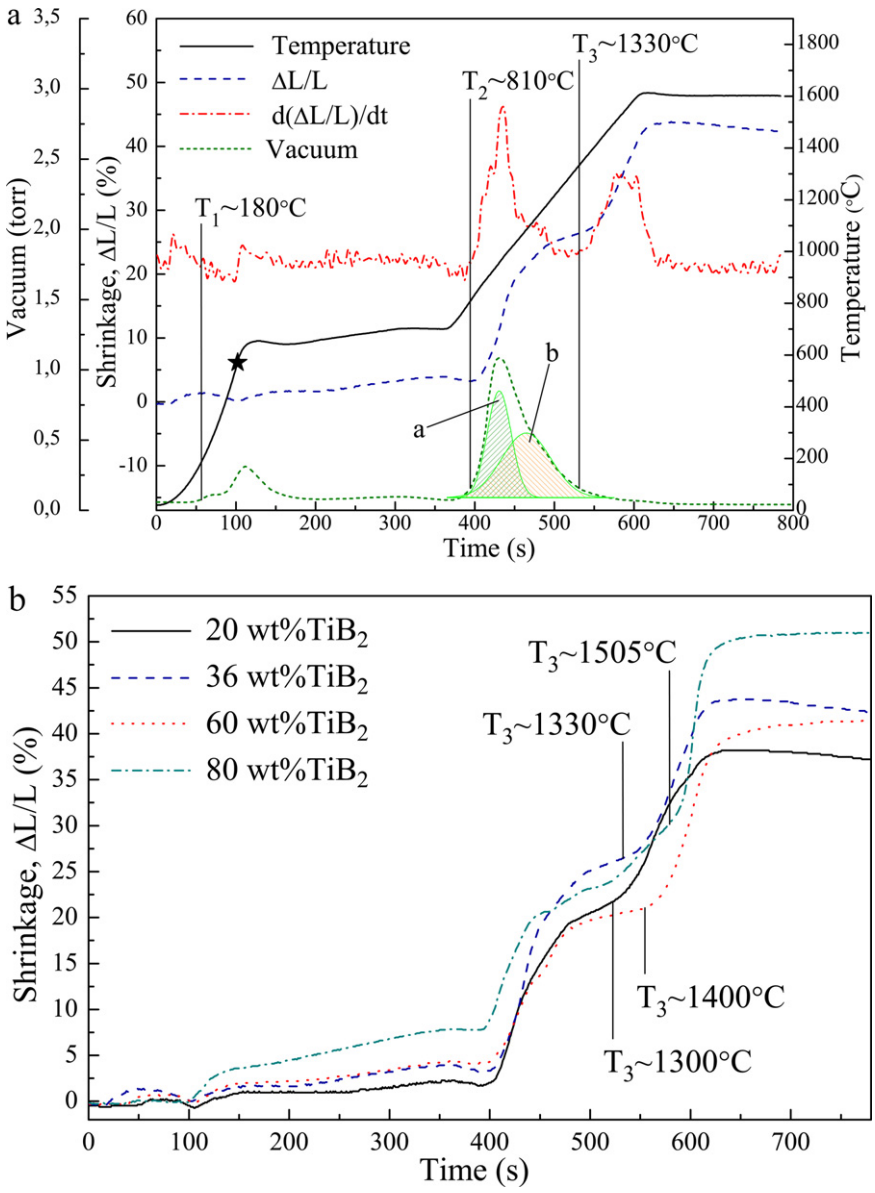

Fig. 1. (a) Shrinkage ($\Delta L/L$) and temperature, shrinkage rate ($d(\Delta L/L)/dt$) in arbitrary units and vacuum level profiles for a sample containing 36 wt% TiB_2 and (b) shrinkage profiles ($\Delta L/L$) for different contents of TiB_2 in sintered samples plotted versus heating time. Sintering was with a heating rate of 225 °C/min. (The asterisk indicates the start of temperature measurement by a pyrometer.)

owing to the exothermic reaction between Ti and B and hence the improvement of the conditions for structure formation. However, the CCs containing 36 wt% TiB_2 have higher maximal shrinkage compared with CCs containing 60 wt% TiB_2. This effect can be attributed to the presence of a higher amount of BN, which is an excellent lubricant in the initial powder mixtures. Typically, at the holding stage (1600 °C) for CCs containing 60 and 80 wt% TiB_2, the shrinkage increases further, in contrast to the decreasing shrinkage for CCs containing 20 and 36 wt% TiB_2 (Fig. 1(b)). Apparently, the complete densification of CCs containing 60 and 80 wt% TiB_2 requires a higher final sintering temperature or a longer holding time. Increasing the TiB_2 content in the sintered CC up to 80 wt% and the heating rate up to 300 °C/min leads to the transient thermal destruction of the graphite die (T_{destr} = 865 °C) as a result of the significant rise in the SHS reaction rate between Ti and B; as well as supported by hydrogen that was generated in the synthesis process.

XRD patterns of CCs densified by RSPS with a heating rate of 225 °C/min as a function of TiB_2 content are shown in Fig. 2. It can be seen that increasing the heating rate to 225 °C/min for CCs with

Table 1
Characteristic temperatures marking the start of synthesis and sintering processes during RSPS.

Heating rate, °C/min	20 wt%TiB_2–80 wt%TiN		36 wt%TiB_2–64 wt%TiN		60 wt%TiB_2–40 wt%TiN		80 wt%TiB_2–20 wt%TiN	
	T_2, °C	T_3, °C	T_2, °C	T_3, °C	T_2, °C	T_3, °C	T_2, °C	T_3, °C
112.5	800	1305	810	1325	805	1395	790	1510
225	790	1300	810	1330	800	1400	785	1505
300	835	1290	835	1320	810	1400	800	–

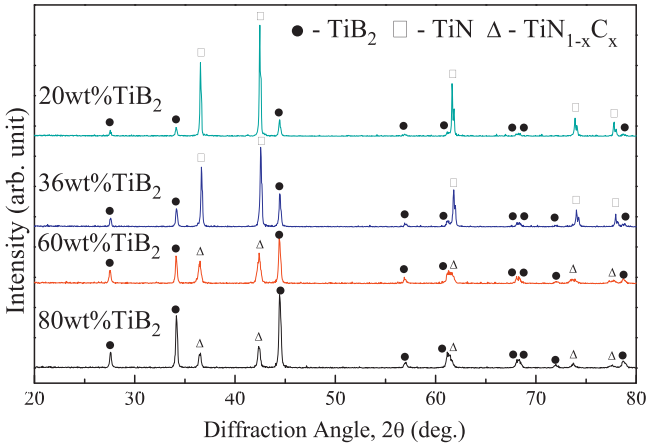

Fig. 2. XRD pattern of CCs densified via RSPS with a heating rate of 225 °C/min as a function of TiB_2 content.

60 and 80 wt% TiB_2 leads to the formation of the nonstoichiometric $TiN_{1-x}C_x$ (x = 0.1–0.3) phase instead of the TiN phase. The formation of the $TiN_{1-x}C_x$ phase occurs on the surface of a sample owing to the diffusion of carbon atoms from the graphite die in the TiN lattice as a result of increasing the heat supply to the system per unit time, as well as by self-heating of the system owing to the exothermic reaction between Ti and B. Increasing the heating rate to 300 °C/min leads to the formation of TiB_2 and $TiN_{1-x}C_x$ phases for all investigated compositions. However, at a relatively low heating rate (112.5 °C/min), only the corresponding TiN and TiB_2 phases were obtained. Moreover, no oxidation products were detected in the sintered CCs even though the sintering temperature was sufficiently high and the vacuum level of the system was sufficiently low (7.5×10^{-2} Torr).

The physical and mechanical properties of the sintered CCs are summarized in Table 2. The highest values of relative density (97.0–97.8%) were obtained for CCs containing 36 wt% TiB_2. The addition of nanocrystalline TiN to the initial powder mixtures results in a decrease in the final density of CCs because of the inertness of TiN in the reaction and its retarding effect on shrinkage (not involved in the synthesis process). The final density of the CCs also decreases with increasing TiB_2 content up to 60–80 wt%. This decrease in density can be explained by competition between phase formation and densification during CC synthesis following the reaction $Ti + 2B \rightarrow TiB_2$ for the TiB_2 lattice and the reaction $3Ti + 2BN \rightarrow 2TiN + TiB_2$ for the TiN/TiB_2. This results in diffusion porosity as well as an incomplete densification process. It should be noted that the maximal density was achieved with the heating rate of 225 °C/min (Table 2).

The hardness of the sintered CCs varies from 16 to 25 GPa and increases slightly with an increase in the amount of the harder TiB_2 phase. The fracture toughness varies in the range of 4–6.5 MPa $m^{1/2}$. Moreover, a heating rate within 112.5–300 °C/min has no significant effect on the mechanical properties of the sintered CCs (Table 2).

The fabrication and properties of the TiN–TiB_2 composites are also reported in many literatures [26–30]. Shobu et al. produced TiN–TiB_2 composites by conventional sintering [26] and hot pressing [27] of TiN and TiB_2 powders. Zhang et al. also prepared these CCs by reactive hot pressing [28] using mixtures of TiH_2 and BN as initial reagents. The selected properties of the sintered TiN–TiB_2 composites are shown in Table 3. Although the relative density of obtained CCs are sufficiently high (98–99%), the described above methods requires much higher sintering temperatures in the range of 1800–1900 °C and relatively longer sintering time (30–90 min) than in the present work. The hardness and fracture toughness are on the same level with that obtained in the present investigation. The reactive hot pressing of Ti and BN mixtures at 1600 °C [29] resulted in not complete densification process (only 88.8% RD) and thus decreasing of hardness to 16.8 (±2.33) GPa (Table 3). Qiu et al. [30] reported about completely conversion of the ball milled Ti + BN powder mixtures to form TiN–TiB_2 using high pressure heat treatment (HPHT) at 1300 °C and 5 GPa. However, the hardness was only 8.84 GPa and no any presented data about density and K_{IC} of that CCs.

Representative SEM images (fractured surface) of the CCs densified via RSPS are shown in. 3. CCs containing 36 wt% TiB_2 have

Table 2
Physical and mechanical properties of sintered ceramic composites.

Composition, wt%	Heating rate, °C/min	Relative density, %	Hardness, HV (GPa)		K_{IC}, MPa $m^{1/2}$
			Load, P = 0.1 kgf	Load, P = 2 kgf	
20TiB_2–80TiN	112.5	96.3	18.9 (±1.03)	17.7 (±0.40)	4.06 (±0.15)
	225	97.0	19.5 (±0.58)	18.0 (±0.58)	4.07 (±0.11)
	300	96.7	21.3 (±1.09)	18.4 (±0.61)	6.16 (±0.70)
36TiB_2–64TiN	112.5	97.7	21.0 (±0.98)	19.8 (±0.29)	4.37 (±0.09)
	225	97.8	20.4 (±1.67)	20.3 (±0.59)	5.05 (±0.17)
	300	97.0	21.5 (±0.91)	19.8 (±0.27)	4.80 (±0.12)
60TiB_2–40TiN	112.5	95.1	22.0 (±1.78)	20.6 (±0.58)	4.74 (±0.15)
	225	96.0	21.5 (±3.68)	19.5 (±0.64)	4.59 (±0.19)
	300	95.3	22.7 (±2.76)	19.2 (±1.84)	5.04 (±0.41)
80TiB_2–20TiN	112.5	93.5	24.7 (±4.40)	24.6 (±3.33)	5.17 (±0.38)
	225	94.2	16.5 (±3.15)	15.9 (±0.66)	6.46 (±0.88)
	300	Destr. at 865 °C	–	–	–

Table 3
Selected properties of sintered TiB_2–TiN ceramic composites.

Composite (fabrication method)	Conditions, (MPa/°C/min)	Density (% RD)/grain size (μm)	Hardness, HV (GPa)	K_{IC}, MPa $m^{1/2}$	Ref.
30 wt%TiB_2–TiN (CS)	–/1900/90	98.0/–	21.0	4.0	[26]
30 wt%TiB_2–TiN (HP)	20/1800/30	~99.0/~3	18.0	3.0	[27]
36 wt%TiB_2–TiN (RHP)	30/1850/30	~98.0/–	18.0	5.8	[28]
36 wt%TiB_2–TiN (RHP)	40/1600/30	88.8/–	16.8 (±2.33)	–	[29]
36 wt%TiB_2–TiN (HPHT)	5000/1300/5	–/0.02–0.04	8.84	–	[30]
36 wt%TiB_2–TiN (RSPS)	80/1600/13	97.8/0.15–0.55	20.4 (±1.67)	5.05 (±0.17)	Present work

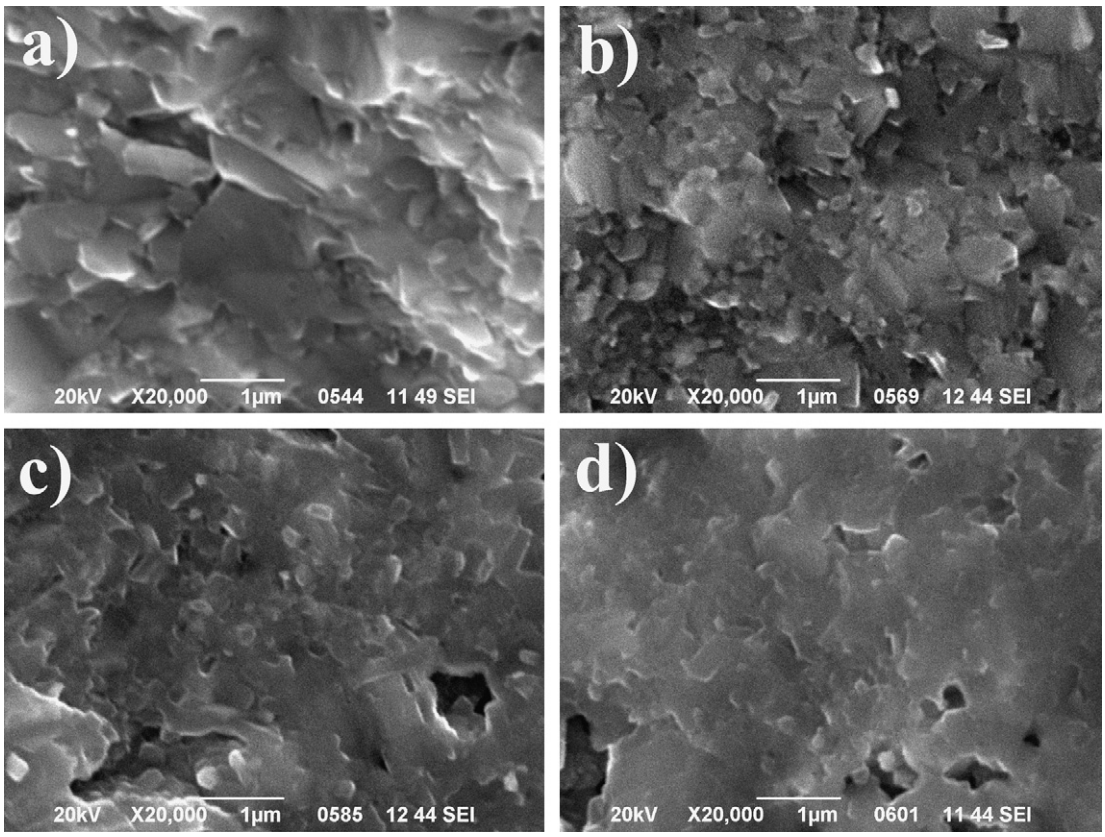

Fig. 3. Representative SEM images (fractured surface) of the CCs densified via RSPS with compositions of (a) 20TiB_2–80TiN, (b) 36TiB_2–64TiN, (c) 60TiB_2–40TiN and (d) 80TiB_2–20TiN (all wt%).

the most homogeneous nanostructure with average grain sizes of 150–550 nm (Fig. 3(b)). The increase in milling time up to 70 h as reported by Qiu et al. [30] could leads to finer microstructure (Table 3); however in case of previous work [30] it was also accompanied by decrease in sintering temperature (1300 °C) that is not the case for present investigation. The hot pressing of TiN and TiB_2 powders [27] leads to the formation of coarser microstructure with average grain sizes of ~3 μm (Table 3). The TiN–TiB_2 composites (20 wt% TiB_2) have nanosize grains (~200–300 nm) as well as relatively large grains (~1–3 μm). The latter can be explained by the presence of agglomerated nanocrystalline TiN in the powder mixture that is not involved in the synthesis process. These agglomerates form large grains during the sintering process (Fig. 3(a)). The nanosize grains those are a result of the synthesis processes (reaction (1)). A further increase in TiB_2 content (60–80 wt%) results in an inhomogeneous structure and an increase in porosity with an average grain size of 300–600 nm (Fig. 3(c) and (d)). The insignificant decrease in the average grain sizes for sintered CCs with increasing heating rates from 112.5 to 300 °C/min was also revealed as a result of a general decrease in the processing time of RSPS.

4. Conclusions

The simultaneous synthesis and densification of TiN–TiB_2 ceramic composites with different component ratios (20–80 wt% TiB_2) under various heating rates via RSPS was performed. It was shown that the omit consolidation process consists of three stages. The first stage is the start of TiH_2 dehydrogenation; the second stage involves SPS-ignited chemical reactions in the system during the most intensive dehydrogenation process; and the third stage is direct sintering of the as-synthesized TiN and TiB_2 components. The temperature increased at the start of the third stage as a result of an increase in the TiB_2 content in the sintered CCs because of the exothermic reaction between titanium and boron. The increase in the heating rate and TiB_2 content in the sintered CCs led to the formation of a nonstoichiometric $TiN_{1-x}C_x$ (x = 0.1–0.3) phase on the surface of the sample instead of the TiN phase owing to the diffusion of carbon atoms from the graphite die in the TiN lattice. The highest relative density (97.0–97.8%) was obtained for CCs containing 36 wt% TiB_2. The hardness of the sintered CCs varied from 16 to 25 GPa; the fracture toughness varied in the range of 4–6.5 MPa $m^{1/2}$. Moreover, the heating rate within the interval 112.5–300 °C/min had no significant effect on the mechanical properties of the sintered CCs. The composites containing 36 wt% TiB_2 had the most homogeneous nanostructure with average grain sizes of 150–550 nm.

Acknowledgments

The authors would like to thank Mr. S. Grasso for his technical support with the SPS system, Dr. C. Hu for his help with SEM work, and Dr. D. Demirsky for his helpful suggestions in the analysis of obtained experimental data.

References

[1] L. Wang, W. Jiang, L. Chen, M. Yang, H. Zhu, J. Am. Ceram. Soc. 89 (7) (2006) 2364–2366.
[2] Y. Han, Y. Dai, D. Shu, J. Wang, B. Sun, J. Alloys Compd. 438 (2007) 327–331.
[3] A. Mukhopadhyay, G.B. Raju, B. Basu, A.K. Suri, J. Eur. Ceram. Soc. 29 (2009) 505–516.
[4] I. Gotman, N.A. Travitzky, E.Y. Gutmanas, Mater. Sci. Eng. A 244 (1) (1998) 127–137.
[5] O. Petukhov, I. Khobta, A. Ragulya, Y. Sakka, Arch. Metall. Mater. 54 (4) (2009) 957–962.
[6] A.M. Locci, R. Orrù, G. Cao, Z.A. Munir, Mater. Sci. Eng. A 434 (2006) 23–29.
[7] J.W. Lee, Z.A. Munir, M. Shibuya, J. Am. Ceram. Soc. 84 (6) (2001) 1209–1216.

[8] S. Grasso, Y. Sakka, G. Maizza, Sci. Technol. Adv. Mater. 10 (2009) 053001.
[9] L.A. Stanciu, V.Y. Kodash, J.R. Groza, Metall. Mater. Trans. A 32 (10) (2001) 2633–2638.
[10] O. Petukhov, O. Derevianko, A. Ragulya, et al., Production method of composite material on the basis of titanium nitride, Ukraine Pat. No. 79526 (2007).
[11] A.I. Raichenko, E.S. Chernikova, E.A. Olevsky, J. Phys. IV C7 3 (1993) 1235–1239.
[12] W. Yucheng, F. Zhengyi, Mater. Sci. Eng. B 90 (2002) 34–37.
[13] V.V. Barzykin, Pure Appl. Chem. 64 (7) (1992) 909–918.
[14] F. Bernard, S. Gallet, N. Spinassou, S. Paris, E. Gaffet, J.N. Woolman, Z.A. Munir, Sci. Sintering 36 (3) (2004) 155–164.
[15] H. Borodianska, L. Krushinskaya, G. Makarenko, Y. Sakka, I. Uvarova, O. Vasylkiv, J. Nanosci. Nanotechnol. 9 (2009) 6381–6389.
[16] H. Borodianska, T. Ludvinskaya, Y. Sakka, I. Uvarova, O. Vasylkiv, Scr. Mater. 61 (2009) 1020–1023.
[17] S. Dobedoe, G.D. Wost, M.H. Lewis, Bull. Eur. Ceram. Soc. 1 (2003) 19–24.
[18] M. Omori, Mater. Sci. Eng. A 287 (2000) 183–188.
[19] O. Vasylkiv, H. Borodianska, Y. Sakka, J. Eur. Ceram. Soc. 28 (2008) 919–927.
[20] O. Vasylkiv, H. Borodianska, P. Badica, Y. Zhen, A. Tok, J. Nanosci. Nanotechnol. 9 (2009) 141–149.
[21] D.K. Shetty, I.G. Wright, P.N. Mincer, P.N. Clauer, J. Mater. Sci. 20 (1985) 1873–1882.
[22] K. Niihara, R. Morena, D.P.H. Hasselman, J. Mater. Sci. Lett. 1 (1982) 13–16.
[23] F. Deniels, R.A. Alberty, Physical Chemistry, second ed., J. Wiley and Sons, New York/London, 1961.
[24] V.S. Zenkov, V.P. Stetsenko, I.V. Khobta, I.I. Timofeeva, A.S. Petukhov, A.V. Ragulya, Powder Metall. Met. Ceram. 46 (9–10) (2007) 492–498.
[25] V.S. Zenkov, A.V. Ragulya, Powder Metall. Met. Ceram. 46 (5–6) (2007) 291–297.
[26] K. Shobu, T. Watanabe, Y. Enomoto, K. Umeda, Y. Tsuya, J. Am. Ceram. Soc. 70 (5) (1987) C-103–C-104.
[27] K. Shobu, T. Watanabe, J. Powder Metall. Soc. Jpn. 32 (6) (1985) 215–218.
[28] G. Zhang, Z. Jin, X. Yue, J. Am. Ceram. Soc. 78 (10) (1995) 2831–2833.
[29] L. Rangaraj, C. Divakar, V. Jayaram, J. Am. Ceram. Soc. 87 (10) (2004) 1872–1878.
[30] L.X. Qiu, B. Yao, Z.H. Ding, Y.J. Zheng, X.P. Jia, W.T. Zheng, J. Alloys Compd. 456 (2008) 436–440.